46th AIAA Aerospace Sciences Meeting and Exhibit
January 7-10, 2008
Reno, NV

AIAA Paper 2008-0230
SAND2007-8151C

Evaluation of PIV Uncertainties using Multiple Configurations and Processing Techniques

Steven J. Beresh*
Sandia National Laboratories, Albuquerque, NM, 87185

Particle image velocimetry (PIV) data have been acquired using three different experimental configurations in the far-field of the interaction created by a transverse supersonic jet exhausting from a flat plate into a transonic crossflow. The configurations included two-component PIV in the centerline streamwise plane at two overlapping downstream stations, as well as stereoscopic PIV in both the same streamwise plane and in the crossplane. All measurement planes intersected at a common line. Data from both two-component measurement stations and the stereoscopic streamwise configuration agreed to within the estimated uncertainty, but data from the crossplane exhibited reduced velocity and turbulent stress magnitudes by a small but significant degree. Subsequent reprocessing of the data in nominally the same manner but using a newer software package brought all values into close agreement with each other, but produced turbulent stresses substantially higher than those from the first software package. The error source associated with the choice of software was traced to the use of image deformation in the newer software to treat velocity gradients, which synthetic PIV tests show yields a more accurate result for turbulence measurements even for gradients within the recommended limits for classical PIV. These detailed comparisons of redundant data suggest that routine methods of uncertainty quantification may not fully capture the error sources of an experiment.

Introduction

The quantification of measurement error is a crucial and necessary component of any instrumentation technique. It is not sufficient to simply report the measured data for given conditions, but essential to additionally provide a reasonable estimate of the range within which the true value may lie. Additional focus upon uncertainty estimation for advanced measurement techniques has emerged due to the increasing commonality of code validation experiments, in which the resulting data are compared to analogous computational results to assess the performance of the numerical model.

The present investigation concerns the use of particle image velocimetry (PIV) to study the far-field of the interaction generated by a transverse supersonic jet exhausting from a flat plate into a transonic crossflow. The far-field of the interaction is dominated by the presence of a counter-rotating vortex pair, which is induced as the jet is turned over and realigned by its encounter with the freestream. Previous publications [1-3] discuss in greater detail the physics of the interaction and the induced vortex pair, whereas the present discussion concerns the accuracy of the data.

To help assess the experimental uncertainty, PIV measurements have been acquired of the same flowfield through three distinctly different configurations. Two-component PIV has been employed in the streamwise plane on the wind tunnel centerline while stereoscopic PIV has been implemented in the crossplane at a single downstream station; these two measurement planes overlap along a common line. Additional data were acquired in the centerline streamwise plane using stereoscopic PIV. The changes between these experimental configurations lead to different manifestations of potential bias errors, allowing a thorough evaluation of experimental error in the measured mean flow properties as well as the turbulent characteristics. Furthermore, two different software

*Principal Member of the Technical Staff, Engineering Sciences Center, Senior Member AIAA, correspondence to: P.O. Box 5800, Mailstop 0825, (505) 844-4618, email: sjberes@sandia.gov

This work is supported by Sandia National Laboratories and the United States Department of Energy. Sandia is a multiprogram laboratory operated by Sandia Corporation, a Lockheed Martin Company, for the United States Department of Energy's National Nuclear Security Administration under Contract DE-AC04-94AL85000.

packages were used to process the data in nominally the same manner, creating another check upon experimental error. Such an approach permits an evaluation not just of the agreement in the data itself, but also of the veracity of the uncertainty estimation.

Experimental Apparatus

Trisonic Wind Tunnel

Experiments were performed in Sandia's Trisonic Wind Tunnel (TWT), which is a blowdown-to-atmosphere facility using air as the test gas through a 305 × 305 mm^2 rectangular test section enclosed within a pressurized plenum. A solid-wall transonic test section was used rather than the traditional ventilated version because it offers reasonable optical access, a flat plate from which the jet will issue, and computationally tractable boundary conditions for comparison of experimental data and numerical simulations. The use of a solid-wall test section limits the Mach number range of the flowfield, but this was considered an acceptable compromise.

Supersonic Jet Hardware

The jet exhausted from a conical nozzle with an expansion half-angle of 15° and an exit diameter d_j of 9.53 mm. The nozzle fit to a settling chamber designed for a maximum pressure of 14 MPa and instrumented to provide stagnation pressure and temperature measurements. Nitrogen was used as the working gas for the jet.

The nozzle mounts along the centerline of the top wall of the test section, which served as the flat plate from which it transversely exhausted. A side-wall window flush with the top wall is positioned downstream of the jet for viewing the far-field of the interaction; a larger window in the pressurized plenum complements the test section window. Windows in the floor of the test section and plenum are located near the position of the side-wall window for introducing the laser sheet. The relative position of the jet and windows within the test section is sketched in Fig. 1, which additionally shows the laser sheets for the PIV measurements and a pressure tap contained in each side wall for measuring the test section static pressure used to determine the freestream Mach number.

Particle Image Velocimetry System

The PIV laser sheet configurations for the jet-in-crossflow experiment in the TWT are shown in Fig. 1. One configuration employed two-component (2-C) PIV in two different streamwise imaging regions on the wind tunnel centerline, where the camera was shifted from an upstream position to an overlapping downstream position to survey a larger streamwise extent of the flowfield. A second configuration acquired stereoscopic (3-C) PIV data to obtain all three velocity components in the wind tunnel crossplane, in which the laser sheet was aligned normal to the wind tunnel axis and positioned to the midpoint of the side-wall window 321.8 mm downstream of the jet nozzle centerline. This position corresponds to 33.8 d_j downstream and lies within the overlap region of the two streamwise planes. A third and final orientation employed stereoscopic PIV in a single streamwise imaging region coplanar with the streamwise regions shown in Fig. 1 and centered upon the 321.8 mm position. Regardless of the PIV configuration, the coordinate system is chosen such that the u component lies in the streamwise direction and the v component is in the vertical direction, positive away from the top wall; the w component is chosen for a right-handed coordinate system. The origin is located at the center point of the jet nozzle exit plane.

The light source for all the PIV measurements was a pair of frequency-doubled Nd:YAG lasers (Coherent Infinity 40-100) that produced about 120 mJ per beam. Streamwise PIV measurements employed a laser sheet 1.2 mm thick and a time between laser pulses of 2.375 μs. The crossplane PIV configuration aligned the freestream direction of the wind tunnel with the out-of-plane motion through the laser sheet; therefore, to limit the resulting particle dropout, a thicker laser sheet of 2.0 mm and a shorter time between pulses of 1.80 μs were employed.

The TWT is seeded by a thermal smoke generator (Corona Vi-Count 5000) that produces a large quantity of particles typically 0.2 - 0.3 μm in diameter from a mineral oil base. Particles are delivered to the TWT's stagnation chamber upstream of the flow conditioning section while the jet itself remains unseeded. Although this creates a serious measurement bias near the jet exit due to selective flow sampling, data acquired further downstream are not subject to such a difficulty because turbulent mixing entrains particles from the freestream and distributes them throughout the interaction once in the far-field. The particles are sufficiently small that they rapidly attain the local velocity once they have been redistributed [4, 5].

Scattered laser light was collected by interline-transfer CCD cameras (Redlake MegaPlus ES4.0/E) with a resolution of 2048 × 2048 pixels digitized at 8 bits. For the 2-C streamwise measurements, a single camera was equipped with a 105 mm lens (Nikon Micro-Nikkor) operating at f/4 and standing 1.1 m from the laser sheet. Given that the angle subtended by the scattered light and the camera axis is small, and that the flowfield is dominated by the streamwise velocity component, perspective error due to the collection angle of the camera lens is expected to be

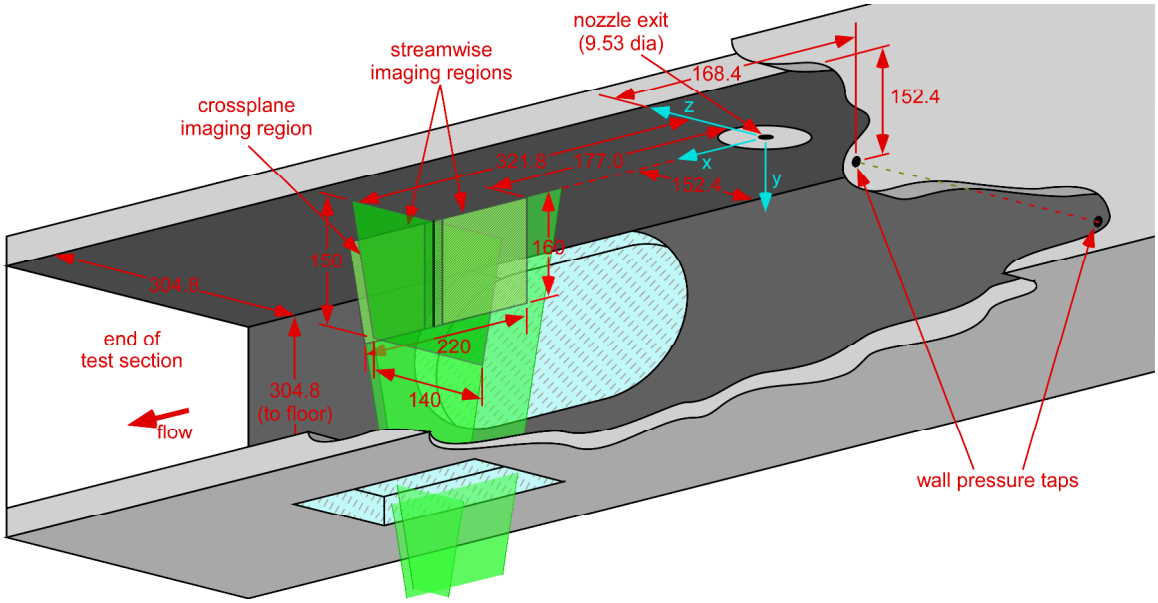

Fig. 1: A schematic of configurations in the wind tunnel for PIV measurements in both the streamwise plane and the crossplane, looking from below the test section in the downstream direction. Flow is from right to left. All dimensions are in millimeters. Not to scale.

minor [6, 7]. The flowfield was surveyed using two separate imaging regions, as indicated in Fig. 1, wherein the camera and laser sheet were relocated to a downstream position for an additional set of wind tunnel runs, constrained by the window positions. An overlap between the two stations ensured complete coverage of the resulting trapezoidal imaging region and also permitted a comparison between measurements at the 321.8 mm position. Calibrations of the 2-C PIV data were accomplished simply by imaging a target placed in the measurement region to convert the object plane length scale to the image plane length scale.

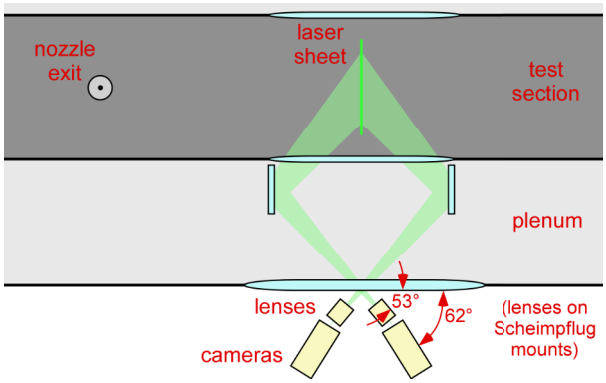

Fig. 2: Schematic of the camera arrangement for stereoscopic PIV for the crossplane configuration. Flow is from left to right.

Stereoscopic PIV used two cameras equipped with 105 mm lenses mounted on Scheimpflug platforms to create an oblique focal plane aligned with the laser sheet. Both cameras looked through the same test section window, viewing the laser sheet from opposite directions, because placing one camera at the other side-wall window precluded access to the test section. To improve upon the limited camera viewing angles, mirrors were rigidly mounted inside the plenum to reflect scattered laser light to the cameras at a sharper angle, as shown in Fig. 2 for the crossplane orientation. This approach allowed an angle of 53° between the camera lenses and the laser sheet normal for the crossplane configuration, or 34° for the 3-C streamwise measurements. The constricted optical access additionally prevents meaningful movement of the crossplane location upstream or downstream; thus all data have been acquired at a single position. The cameras were configured similarly for the 3-C streamwise imaging region; this location was principally intended to provide comparative data at the 321.8 mm downstream position. Stereoscopic camera calibrations used the multi-plane procedure described by Soloff et al. [8] to tie together the two sets of image pairs to produce three-dimensional vectors.

Data initially were processed using IDT's ProVision 2.02, but a later purchase of LaVision's DaVis 7.1 allowed reprocessing of the same images using the newly available algorithms. Regardless of the software, for both the 2-C and the 3-C PIV, image pairs were interrogated with a 64 × 64 pixel window employing two iterations with adaptive window offsets to account for the local particle displacement, and the LaVision software additionally incorporates image deformation based upon local velocity gradients, using a bilinear interpolation scheme to warp the images.

The relatively large interrogation window was chosen to favor precision over spatial resolution, appropriate to a data set intended for code validation. The spatial resolution of the 2-C PIV was 5.0 × 5.0 mm^2, but for the crossplane configuration, the spatial resolution varies across the image due to the oblique camera view, yielding 9.3 mm horizontally and 5.9 mm vertically, measured at the wind tunnel centerline. The 3-C streamwise configuration had a spatial resolution of 6.2 mm horizontally and 5.4 mm vertically, measured at the 321.8 mm position. An approximate 50% overlap in the interrogation windows was typically used as well to oversample the velocity fields. The resulting vector fields were validated based upon signal-to-noise ratio and nearest-neighbor comparisons.

Experimental Conditions

The freestream Mach number is M_∞=0.8 with a wind tunnel stagnation pressure P_0=154 kPa, which yields a test section static pressure p_w=101 kPa. The nominal stagnation pressure for the Mach 3.73 jet is P_{0j}=4.96 MPa, producing a nominal jet-to-freestream dynamic pressure ratio J=10.2. Additional cases span a range of J values while maintaining M_∞=0.8 to examine the impact of varying the relative strength of the jet, but P_{0j} was chosen such that the jet was always overexpanded. The wall pressure p_w was measured from the static pressure taps on the wind tunnel side walls 168 mm upstream of the jet nozzle centerline, as seen in Fig. 2. M_∞ and the velocity reference U_∞ were calculated isentropically from the ratio p_w/P_0 and the stagnation temperature T_0. The gas supply for the jet was unheated, so the jet stagnation temperature T_{0j} varied from 296 K to 307 K depending upon the laboratory ambient conditions. The wind tunnel air supply is heated in the storage tanks, but not temperature-controlled subsequent to this; therefore the freestream stagnation temperature T_0 also is subject to slight variation from 324 K to 329 K.

The 99%-velocity boundary layer thickness has been measured as 15.4 ± 0.4 mm from PIV data acquired in the streamwise plane [1]. This measurement was made on the wind tunnel centerline at the same downstream position as the crossplane laser sheet (321.8 mm).

The quantity of data that were acquired varied depending upon the PIV configuration and the test conditions. The 2-C PIV measurements acquired sufficient data for reasonable convergence of turbulence quantities in all cases, though many more image pairs were collected for J=10.2 (about 3000). For stereoscopic PIV, a data quantity adequate for turbulent properties was gathered only for J=10.2 (4000 image pairs per camera), with the remaining three cases intended for mean data only.

Results and Discussion

Velocity Fields

The mean velocity data from the 2-C PIV in the streamwise plane are presented in Fig. 3 for the M_∞=0.8 and J=10.2 case, combining the measurements from both imaging stations and displaying the streamwise velocity component u and the vertical velocity component v as separate contour plots. These data were originally reported in Beresh et al. [1], where numerous other cases may be found as well. Distances are normalized to d_j and velocities to U_∞. Figure 3 shows that the jet penetration and trajectory are readily discernable from the velocity field. The deficit in u tracks the position of the jet from its impedance of the oncoming crossflow, whereas the increase in v marks the location of the counter-rotating vortex pair due to the induced vertical velocity component. The decay of the jet and vortex strength with downstream distance is apparent by the decrease in the magnitudes of the velocity deficit in u and vertical velocity v in each case, while simultaneously the penetration of the jet and vortices into the freestream is tracked. The gradual increase in freestream values of u in the streamwise direction occurs because the increased jet penetration and the wall boundary layer growth reduce the effective wind tunnel freestream area and hence increase the local Mach number. An artificial reduction in velocity can be observed in the upper left corner of each contour plot and along the inclined downstream edge of the measurement region, owing to proximity to an edge of the laser sheet. Similarly, the vertical seams visible are an artifact of having combined data from two distinct camera positions; these incongruities lie within the uncertainty of the measurements.

The vortex structure is much better examined from the crossplane 3-C PIV data, shown in Fig. 4 for the same conditions as Fig. 3, reproducing data from Beresh et al. [3]. In-plane velocities are displayed as vectors superposed upon a contour plot of the out-of-plane (streamwise) velocities. Again, axes have been normalized to d_j and velocities to U_∞. The vector field in Fig. 4 clearly shows the counter-rotating vortex pair, which is centered near the lower portion of the streamwise velocity deficit shown by the contours, consistent with observations from the streamwise data. Strong streamwise velocity deficits near the wall within the boundary layer indicate the remnant of the horseshoe vortex that forms around the jet plume immediately after exit from the nozzle.

The streamwise 3-C PIV measurements are not shown because they add little to Fig. 3, as the mean w-component of velocity is essentially zero at the wind tunnel centerline (evident in Fig. 4).

Turbulent fluctuations are easily found by subtracting the mean velocity fields from each instantaneous vector

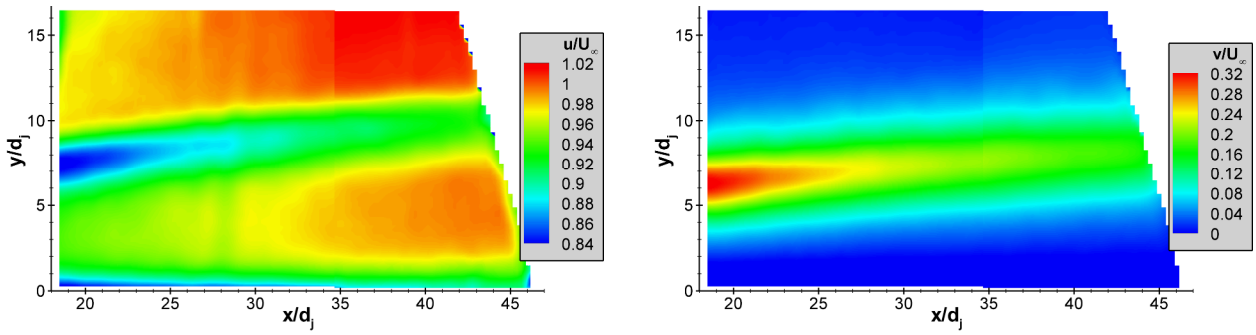

(a) **(b)**

Fig. 3: Mean velocity field of the streamwise two-component PIV data for M_∞=0.8 and J=10.2. (a) streamwise component; (b) vertical component. From Ref. [1].

field, from which the turbulent stresses can be computed. In the case of the 2-C data, this produces two turbulent normal stresses $\overline{u'^2}$ and $\overline{v'^2}$ and one turbulent shear stress $-\overline{u'v'}$; the 3-C configurations yield all six unique components of the Reynolds stress tensor. Due to space constraints, turbulent quantities are not shown in the present document, except comparatively between PIV configurations as discussed below. An extensive discussion of the streamwise turbulent properties is found in Beresh et al. [2] and the crossplane turbulence in Beresh et al. [3].

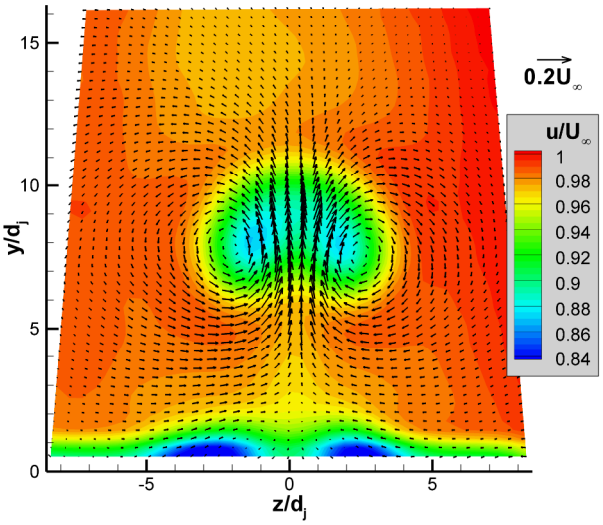

Fig. 4: Mean velocity field from the crossplane stereoscopic PIV data for M_∞=0.8 and J=10.2. From Ref. [3].

Uncertainty Analysis

The uncertainty of the mean velocity measurements consists principally of bias error in the PIV calibration (i.e., registration error) and precision error due to correlation noise, experimental repeatability, and data convergence error. The precision uncertainty is straightforward to determine from the scatter between measurements conducted with an identical calibration, both within a single wind tunnel run and between multiple runs. For the 2-C PIV, the data for the J=10.2 case were acquired over a number of days employing multiple calibrations, and therefore the calibration uncertainty may be estimated by computing the scatter between mean data measured using nominally identical calibrations. Combining these two error sources shows that the uncertainty estimate for the mean velocity data, defined as the 95% confidence interval, is a maximum of about ±7 m/s in each of the u and v components, or 0.025 U_∞. The typical uncertainty in J is ±0.1 and in M_∞ is ±0.002, which are partly responsible for the mean velocity field uncertainties. Uncertainties in the turbulent quantities were determined similarly. Calibration bias was found to exceed precision uncertainty, except for the turbulent stresses where convergence of the data is more significant. In this latter case, convergence error was isolated and reduced in a √N manner by the number of constituent wind tunnel runs; more details are found in Beresh et al. [2].

Uncertainties for the 3-C PIV measurements necessarily must be estimated differently, as only a single calibration was performed for each of the two configurations. The repeatability and convergence of the mean measurements were assessed using multiple wind tunnel runs for the J=10.2 case, from which the precision uncertainty was found as the 95% confidence interval of the scatter in the measurements, again including the effect of variations in J and M_∞. The bias component of the error could not realistically be estimated through repeated calibrations, as was accomplished for the 2-C measurements, partly owing to the difficult and time-consuming nature of the process and partly because the calibration bias is substantially reproducible. Instead, the calibration bias was found by reinstating the calibration target into the measurement location and traversing it a known distance in two dimensions corresponding to the expected particle motion in the time between laser pulses, then processing

the resulting images as if they were PIV data. Bias values were found from the deviation of the measured translation with the actual motion. Because the target was aligned to the wind tunnel in the same fashion as for acquiring calibration images, this procedure accounts for biases produced by the calibration algorithm and not those arising from a misalignment with the actual laser sheet position. Combining all enumerated error sources, uncertainties in the 3-C crossplane measurements were calculated as ±9 m/s, ±4 m/s, and ±6 m/s in the *u*, *v*, and *w* components, respectively, which equate to $0.03U_\infty$, $0.015U_\infty$, and $0.02U_\infty$, respectively.

The precision portion of the stereoscopic turbulent stress uncertainties was determined in the same manner as the mean velocity uncertainties, by examining the deviation between multiple wind tunnel runs. The effect of the calibration bias upon turbulent quantities is somewhat more complicated, as additive bias errors will subtract out when the turbulent fluctuations are calculated, but multiplicative biases will not. To be conservative, the entire bias error is assumed to be multiplicative and the same scaling error seen over the mean velocity range applies to the velocity fluctuations. Still, the calibration bias error affects the turbulent stresses less than the mean velocities because the fluctuation magnitudes are smaller than those of the mean velocities.

Additional wind tunnel runs were conducted for both the 2-C configuration and the 3-C crossplane configuration in which the time between laser pulses was steadily increased from the standard value. Reasonable changes to this parameter did not significantly alter the results, indicating that out-of-plane motion did not induce a bias error by selectively removing some particles from the PIV correlations.

Data Comparisons

The streamwise and crossplane measurement configurations intersect at a common line on the wind tunnel centerline 33.8 d_j downstream of the jet nozzle centerline. To compare the results from the three PIV configurations, mean velocity data from the four test cases of varied *J* were extracted along this line and are shown in Fig. 5 on separate plots for the *u* and *v* components. Four curves are given for each case: each of the upstream and downstream positions for the 2-C PIV in the streamwise plane, the 3-C PIV in the crossplane, and the 3-C PIV in the streamwise plane. Sample error bars are provided based upon the uncertainty analysis detailed above. These error bars appear relatively large because the far-field velocities induced by the jet are a small fraction of the freestream velocity. The reduction of error for the in-plane velocity components of stereoscopic measurements as compared to the 2-C error results from the contribution of two velocity correlations, one from each camera [9]. For the 3-C crossplane configuration, the uncertainty in *u* is more than twice that in *v*, contrary to analyses that predict a lower uncertainty for *u* at the present camera angle [9, 10]. This is because these analyses neglect the effect of calibration bias; in fact, in the present case, the out-of-plane error in the stereoscopic measurements was found to be dominated by such biases.

In all cases in Fig. 5, the 2-C PIV measurements from the two streamwise stations agree to within their uncertainty. This is generally not the case concerning the stereoscopic crossplane configuration. In both *u* and *v*,

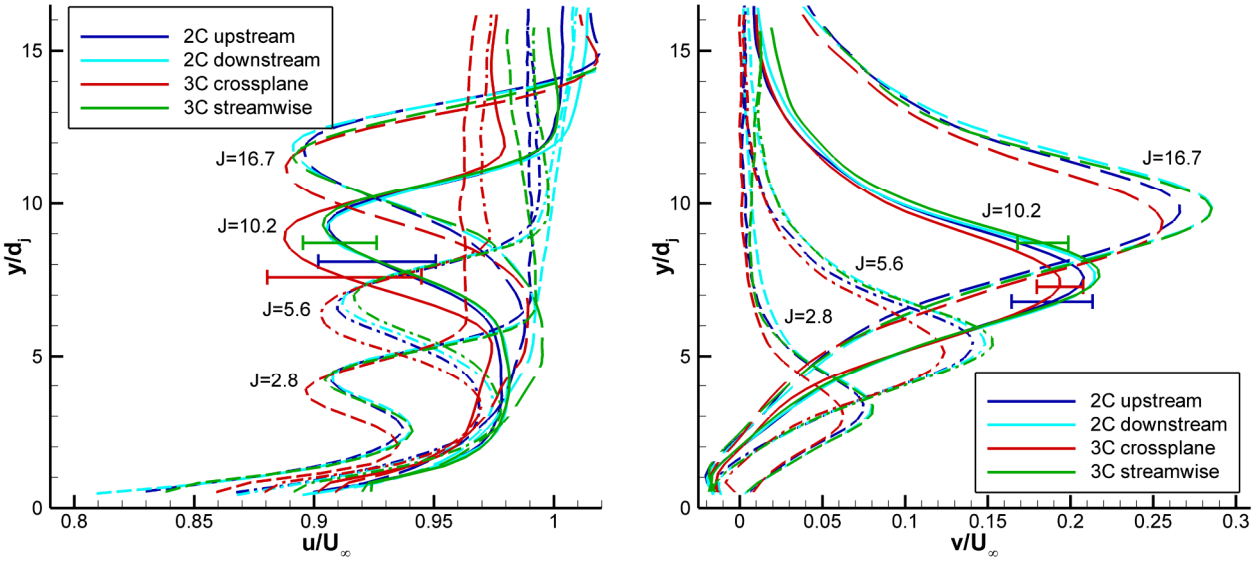

Fig. 5: Comparison of mean velocity profiles common to all PIV configurations along a line of intersection 321.8 mm downstream of the jet. (a) streamwise velocity; (b) vertical velocity.

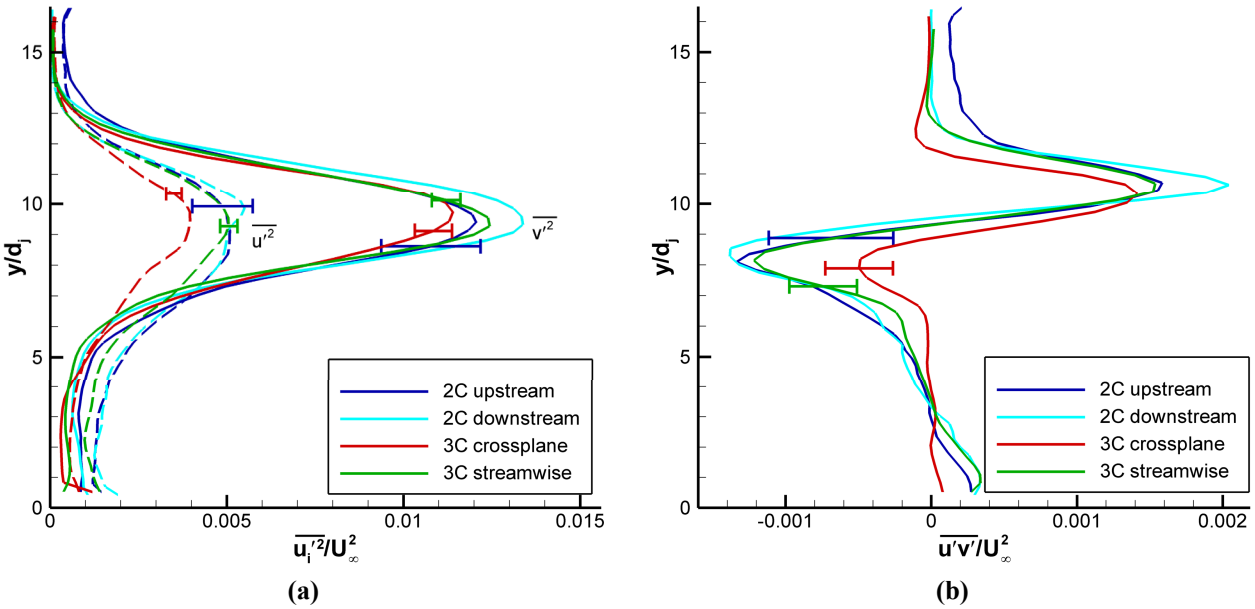

Fig. 6: Comparison of turbulent stress profiles common to all PIV configurations along a line of intersection 321.8 mm downstream of the jet. (a) normal stresses; (b) shear stress.

the crossplane data consistently lag the other three curves. In the case of *u*, the uncertainty is relatively large because this velocity component is aligned to the out-of-plane direction and thus the crossplane measurements still can be said to agree with their counterparts; however, the error bar for the *v* component is appreciably less and the crossplane data fall slightly short of one or more of the other configurations. It is unlikely that this discrepancy is isolated to the one particular calibration used for the crossplane data shown here, as such error should be present in the quantification of the bias error described above, and furthermore, a small set of measurements acquired using a different alignment and calibration closely matched the crossplane data shown in Fig. 5. The stereoscopic streamwise data, on the other hand, are in close agreement with the two 2-C curves for both *u* and *v*. In analyzing these data comparisons, it is important to remember that the uncertainty bars do not indicate a range within which all values are equally likely; rather, values well within the bars are appreciably more probable than values near the outer range of the bars. Thus, to account for the reduced magnitude in the crossplane data, both the crossplane and the streamwise stereoscopic measurements would require errors in the *v* component nearly at the 95% confidence level, which has a low probability.

A comparison of the turbulent stresses is shown in Fig. 6, though only for the three stress components that were measured by all the PIV configurations, and only for the J=10.2 case in which sufficient data were gathered to compute the turbulent quantities. As in Fig. 5, the two stations for the 2-C streamwise configuration agree to within their (relatively large) uncertainty, and the stereoscopic streamwise configuration also agrees well with these data. However, the crossplane data possess an appreciably smaller magnitude than the other three curves, frequently by a value in excess of the error bars; this is consistent with the similar discrepancies in the mean velocity data and indicates that the source of these disagreements does not cancel out when the turbulent fluctuations are calculated.

The comparisons indicate that all data acquired in the streamwise plane, whether 2-C or 3-C, agree within the estimated measurement uncertainty, but that the 3-C crossplane data deviate from the other configurations by an amount slightly exceeding the uncertainty. As this difference is small, it is tempting to regard it as relatively unimportant, but the point of the present study is to make several independent measurements complete with uncertainty estimation, and to then assess their agreement. This discrepancy, then, is significant despite its limited magnitude and suggests that some error occurred specific to the crossplane configuration and not the stereoscopic PIV generally. This does not necessarily indicate that the 3-C crossplane data are flawed, but that the associated uncertainty estimate is insufficient to explain the measurement disparity. Perhaps the most likely source of the discrepancy is an alignment error between the calibration target and the laser sheet position. A similar stereoscopic crossplane configuration in Van Doorne et al. [11] found calibration biases significantly greater than the measurement precision, and although Willert [12] did not use a multi-plane calibration, he similarly detected a large degree of calibration error arising from mild target misalignment.

Another possibility to consider is that actual flowfield differences account for the measurement inconsistency,

given that data from the various PIV configurations were acquired many months apart. However, the 2-C measurements were conducted over a time frame exceeding one year, in which the experiment (instrumentation as well as wind tunnel hardware) was removed and reassembled on three occasions. All such data remained well within the uncertainty, as did a repeat of the crossplane measurements using a different PIV construction several months later. These repeated experiments demonstrate the robustness of the experiment.

All the data shown thus far have been processed using IDT's ProVision software. At a later point in time, the analysis software used in the laboratory was shifted to LaVision's DaVis, which created the opportunity to reprocess the current data. Initially, this was done principally as a training exercise for the new software, but DaVis also possesses the relatively new self-calibration feature, in which correlations between cameras at the same time instance are used as a correction for misalignment between the calibration plane and the laser sheet [13]. Reprocessing the data using this feature potentially could resolve the cause of the discrepancies of the crossplane measurements as compared to those from the streamwise plane.

Instead, data processed using LaVision's DaVis under nominally identical parameters and employing the same calibration showed appreciable differences from the earlier IDT results. This is evident in Fig. 7, in which the mean velocity profiles at the line of intersection of the measurement planes are shown to compare the IDT and LaVision results; the downstream 2-C station and the streamwise 3-C data are omitted to reduce clutter, as their presence is not necessary to the following observations. Uncertainty bars for the LaVision results were found identically to those for IDT as described earlier, but use the newly reduced values and hence reach different error estimates. The agreement between the 2-C streamwise and the 3-C crossplane measurements is appreciably better for the LaVision results than for IDT when examining the vertical component in Fig. 7b, where the crossplane results from LaVision do not display the reduced magnitude observed for the IDT results. In fact, analysis has shown that the in-plane 3-C calibration bias discussed earlier is dramatically less (nearly an order of magnitude) for the LaVision data. Although the streamwise component in Fig. 7a still shows a somewhat lagging velocity for the crossplane measurement regardless of the software utilized, this difference falls within the measurement uncertainty. This improved agreement occurred without the use of the self-calibration feature, suggesting that the data discrepancies found in the IDT results have some other cause.

More alarmingly, the comparison of the corresponding turbulent normal stresses in Fig. 8a shows that results from each of the two software packages disagree with each other by about 20% for the vertical component and almost 50% for the streamwise component, with the LaVision software producing larger values; the turbulent shear stress in Fig. 8b shows a somewhat larger magnitude for LaVision as compared to IDT, but this cannot be considered significant in light of the uncertainty bars. Even for the large discrepancies in Fig. 8a, agreement between the streamwise and crossplane data for either software package is within the uncertainty; it is the difference between software packages themselves that is cause for concern. Considering that any flaws or limitations within the data itself should be replicated when processed by either software package, the difference between the IDT and

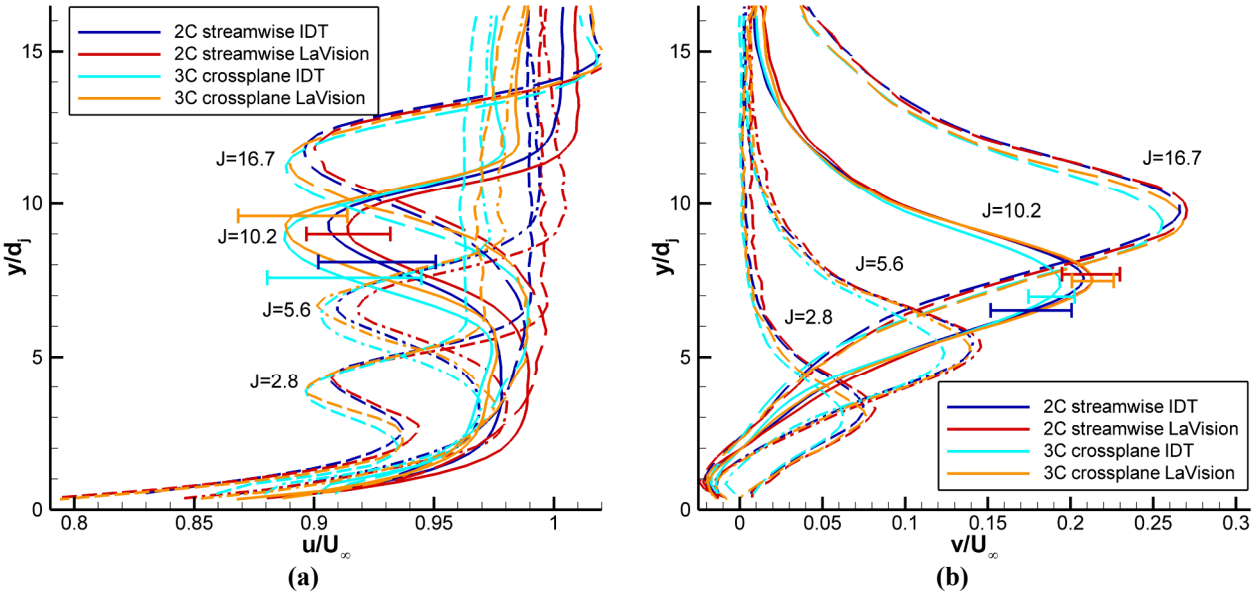

Fig. 7: Comparison of mean velocity profiles as processed by IDT's ProVision or LaVision's DaVis software. (a) streamwise velocity; (b) vertical velocity.

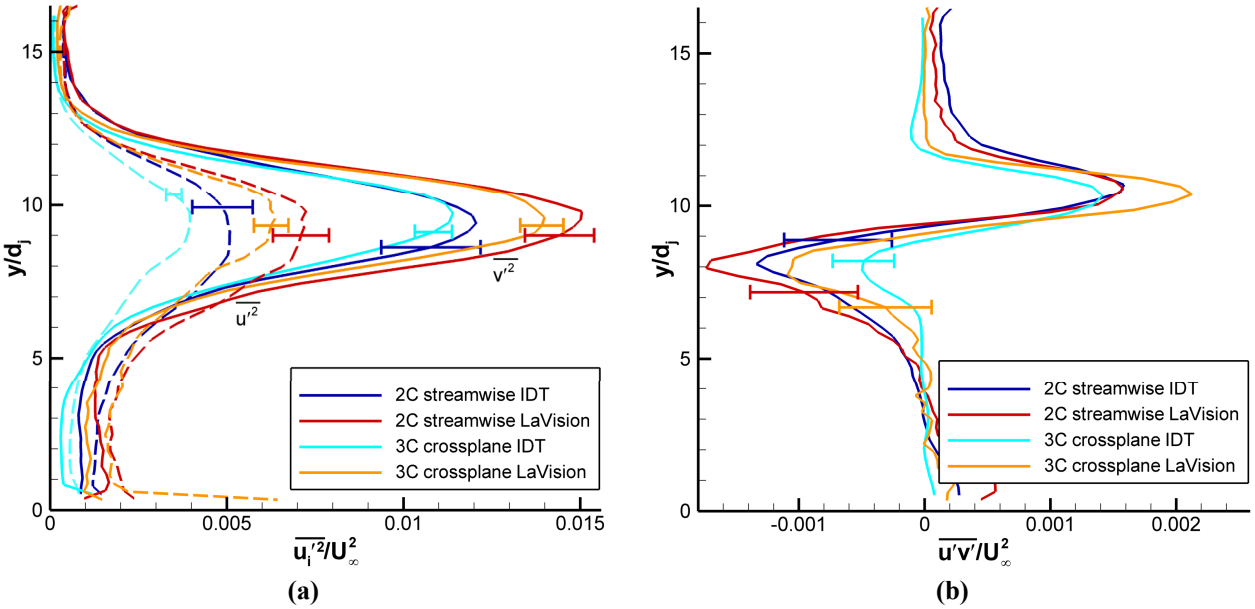

Fig. 8: Comparison of turbulent stress profiles as processed by IDT's ProVision or LaVision's DaVis software. (a) normal stresses; (b) shear stress.

LaVision results indicates the potential for a serious error.

The most obvious possibility for the software-related difference in turbulent stresses is peak locking, particularly because the particle image diameter in the present experiments is near one pixel (unavoidable due to the small particle size needed to track the flow and the low energy of the side-scattered laser light) and is therefore more subject to this difficulty [14, 15]. Differences in the data processing algorithm conceivably could yield different peak-locking effects, as the LaVision software incorporates image deformation, which has been shown to reduce peak locking errors [16-19], and the IDT software does not. Christensen [20] indicates that even extreme peak locking has no discernable effect upon the mean but may seriously bias turbulent fluctuations. However, velocity histograms, such as shown in Fig. 9, reveal minimal peak locking for the present work, even for the IDT software lacking the deformation feature, and Christensen's [20] results show that the level of error found in Fig. 8 would require a rather dramatic peak-locking effect. Furthermore, the valid vector rate is virtually identical for data processed by both software packages and exceeds 99% at the x/d_j=33.8 line of intersection, so a selective vector dropout does not account for the bias.

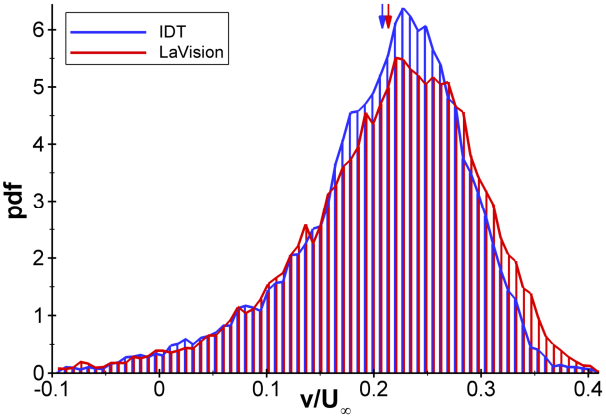

Fig. 9: Probability distribution functions for the vertical velocity component at a point y/d_j=9.5 (the $\overline{v'^2}$ peak in Fig. 8a) in the 2-C streamwise data for IDT's ProVision and LaVision's DaVis software. The arrows indicate mean values.

The velocity histograms also are illustrative of how an apparently mild difference in the velocity distribution produces a much more substantial impact on the turbulence intensity. Figure 9 shows probability density functions of the vertical velocity component at the location of its peak value in Fig. 8, taken from the 2-C PIV data for both IDT and LaVision data processing; hence, these are distributions at a single point in the flow. The arrows in Fig. 9 indicate the mean value of v/U_∞. The figure shows that the IDT distribution has a greater probability of occurrence of velocities near the mean (i.e., it has a larger peak) whereas the LaVision distribution is more likely to yield a value well above the mean (i.e., the broader positive edge of the profile). Qualitatively, this difference appears slight, but once the turbulence intensity is computed, the cumulative effect of the IDT software concentrating more velocities near the mean as compared to the LaVision software results in about a 25% difference in $\overline{v'^2}$. Of course,

at this point, it is not yet clear what accounts for the difference in velocity distributions, much less which result is correct.

Synthetic PIV

In an effort to resolve the discrepancy between the IDT and LaVision results, the well-established tactic of synthetic PIV images was employed. Sets of 1000 image pairs of 256 × 256 pixels each were generated for 2-C analysis, but velocimetry results were obtained only for the interior of the images such that no edge effects occurred. One-dimensional turbulence was simulated by assigning a unique, non-integer streamwise displacement to each image pair, such that every particle in that image pair possessed the identical displacement. Displacements were randomly chosen for each image pair using a Gaussian distribution of some assigned width σ_v, whose magnitude establishes the simulated turbulent intensity, then the correct velocities were recorded for later comparison with the PIV analysis. Particle images were created with a Gaussian intensity distribution of fixed width and particle locations were randomly chosen centered at subpixel values. Various particle diameters and seeding densities were tested to represent different seeding conditions. Shown in this document are three cases: a particle image diameter of $d_p \approx 3$ pixels seeded at a mean density of ten particle pairs per interrogation window with image saturation at half the maximum particle intensity; $d_p \approx 1.5$ pixels with a much higher seeding density and no saturation except when particle images overlap; and $d_p \approx 1.0$ pixels at similar conditions. The real PIV data that are the focus of this paper lie somewhere between the latter two cases. Other particle sizes and seeding parameters were examined and the results found to be consistent with the forthcoming conclusions.

The results of processing the synthetic PIV images with both the IDT and LaVision software are shown in Fig. 10, where Fig. 10a displays the error in the mean over the 1000-image-pair set (the mean is nominally zero, but not precisely) and Fig. 10b gives the error in the streamwise turbulent stress. Neither the mean nor the turbulent stress displays error that is a meaningful function of the simulated turbulent strength. Only the $d_p \approx 3$ data as processed by IDT shows much variation with σ_v, and this is probably convergence error for the mean and additional noise in the turbulent stress due to difficulty in locating the correlation peak for a large, saturated particle image [14, 15]. The LaVision software returns significantly better results for these relatively large particle images, which can be attributed to its use of sub-pixel window offsets [18, 19], though this case still produces a larger error in the turbulent stress than any other LaVision result. Excepting the $d_p \approx 3$ case, which is not the best representation of the real data in this study, the errors in the mean velocity are less than 0.001 pixel and in the turbulent stress less than 0.01 pixel, and therefore are inadequate to explain the discrepancies of Figs. 7b and 8a.

Numerous studies have demonstrated the advantages of image deformation in the analysis of flows with strong velocity gradients [17, 18, 21-24]. The additional correlation noise due to velocity gradients has been recognized since the infancy of PIV [25] and is caused by the simultaneous broadening of the correlation peak and the reduction of its amplitude as non-identical particle displacements are summed within an interrogation window. Bias errors can be even more pernicious and arise from at least two sources: Westerweel [14] describes the mathematical bias towards zero displacement that occurs due to the skewing of the correlation peak when employing cyclic FFT algorithms for cross-correlations, as is most often the case in PIV analysis; and Lecuona et al. [23] discusses the group-locking phenomemon, in which velocity gradients that vary within an interrogation window introduce an

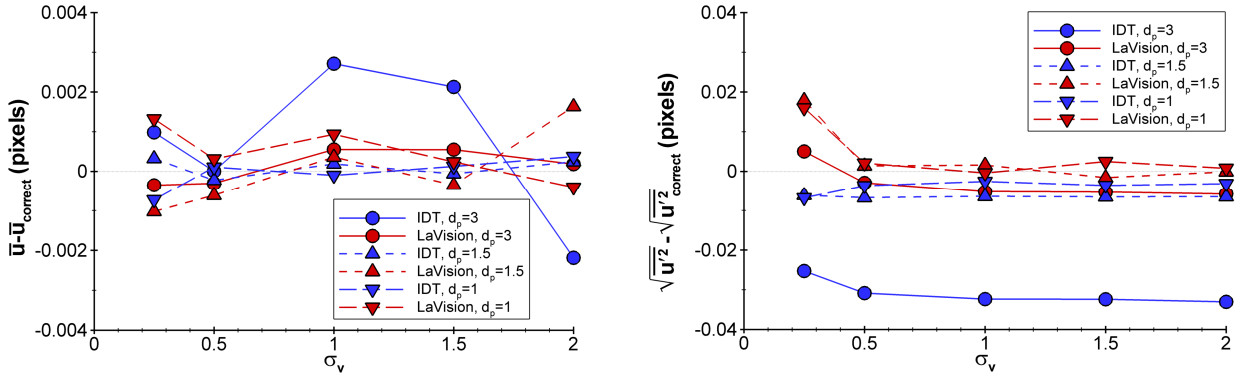

(a) **(b)**

Fig. 10: Error in synthetic PIV images of one-dimensional turbulence as processed by IDT's ProVision or LaVision's DaVis software as a function of the magnitude of the simulated turbulent intensity. (a) mean velocity; (b) turbulent stress.

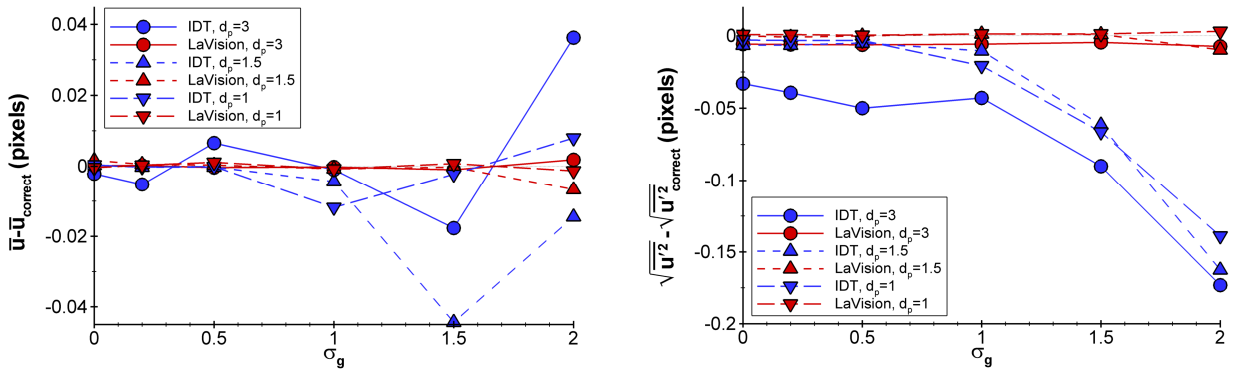

(a) **(b)**

Fig. 11: Error in synthetic PIV images of one-dimensional turbulence with an imposed linear velocity gradient as a function of the magnitude of the simulated gradient distribution (σ_v =2.0). (a) mean velocity; (b) turbulent stress.

additional bias. Therefore, velocity gradients must be added to the synthetic PIV in order to seek meaningful differences in the performance of the two software packages.

To approach this matter, the simulated one-dimensional turbulence was modified to include an additional parameter σ_g, which describes the width of a Gaussian distribution of velocity gradient strength. For each image pair, the velocity strength first is randomly selected based upon σ_v, same as previously, but then a linear gradient across the image is imposed whose magnitude is randomly chosen using σ_g in an identical fashion to the selection of the velocity magnitude. Figure 11 shows the results from each software package as a function of σ_g when σ_v is fixed at 2.0, displaying a clear, significant difference in the turbulent intensity error for the two analyses. The mean error is very small and invariable with respect to σ_g for the LaVision results, but the IDT data become more erratic as the gradient strength rises, probably as a result of convergence error for increasingly noisy results. The error in the turbulent stress is particularly revealing; again, the error in the LaVision results is low and constant, but here the error in the IDT results increases markedly as the gradient becomes stronger and reaches a magnitude of nearly 0.2 pixels, a substantial measurement bias. The bias direction is negative, which is consistent with the real data of Fig. 8a displaying a reduced turbulent stress for IDT results as compared to LaVision. Clearly, the image deformation algorithm of LaVision successfully reduces error resulting from velocity gradients. This is not a result of improved sub-pixel precision, although image deformation does help in this regard [16-18], but because classical algorithms filter out relevant velocity information that image deformation successfully retrieves [17, 21, 23]. In fact, Lecordier and Trinité [26] show that this loss of information can lead to precisely the velocity histogram distortion observed in Fig. 9.

It is interesting to further note that Fig. 11 indicates that the LaVision results are not a significant function of the particle image diameter, even though Astarita and Cardone [27] show that most choices of subpixel interpolation scheme return error levels of about 0.1 pix as d_p becomes small enough. It therefore would be anticipated that particles of about d_p=1 simply do not provide sufficient information for a meaningful interpolation between pixels and in this case image deformation is not useful; some support for this conjecture is found from case A of the Second PIV Challenge [24]. In the present case, both for the synthetic PIV and the real data that it represents, the particle density is quite large and particle images commonly overlap. This creates structures in the images with characteristic lengths exceeding a single pixel, and therefore larger values for the corresponding size of the patterns upon which the software correlates.

Having established that the presence of velocity gradients leads to turbulent stress bias errors in the IDT results but not the LaVision results, it is necessary to ask if those gradients found in the real data are sufficiently large to generate errors consistent with Fig. 8a. Keane and Adrian's [28] classical analysis recommends a maximum allowable pixel displacement due to the velocity gradient of no more than 3% of the interrogation window width, though Lecuona et al. [23] recognize that the maturation of PIV has led to application in more demanding flowfields and in fact advanced processing algorithms such as image deformation allow Keane and Adrian's criteria to be exceeded. Westerweel [14] provides a more specific guideline, also for classical PIV, that the velocity gradient not exceed the ratio of the particle image diameter to the interrogation window width, which he notes is ordinarily about 3-5% and hence consistent with Keane and Adrian [28].

Referring to Fig. 11b, the bias error for the IDT analysis starts to become noteworthy when σ_g=1.0, which

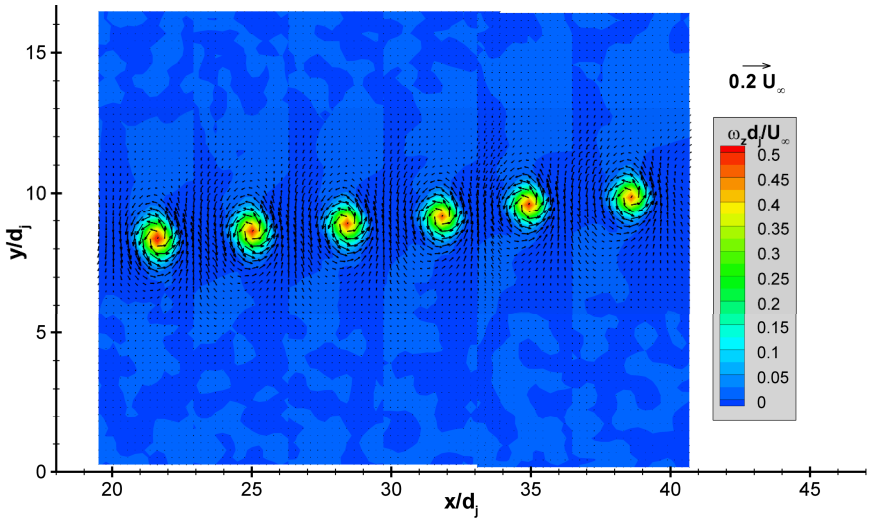

Fig. 12: Representative large-scale turbulent eddies of positive vorticity at six locations found by conditional ensemble averaging for M_∞=0.8 and J=10.2. From Ref. [2].

corresponds to a mean velocity gradient of 0.5% of the interrogation window width (64 pixels) with 95% of the individual image pairs lying below a 1.7% gradient. This simulated condition lies within Keane and Adrian's recommendation. When σ_g=2.0, the mean velocity gradient is 1% with 95% of the data set below 3.5%. Although this reasonably meets the same criteria, Fig. 11 clearly shows that the classical PIV analysis performed by the IDT software yields significant error in the turbulent stress (though the error in the mean velocity is more tolerable). This could be due to bias error arising in those few image pairs in which the velocity gradient exceeds the criteria, or, as suggested by Fig. 9, relatively mild errors in velocity may lead to much more significant errors in the turbulent stress if they occur at some distance from the mean.

The corresponding maximum mean velocity gradient in the vertical direction from the 2-C streamwise data of Fig. 3b is about 0.4% at the downstream position plotted in Figs. 5-8, also well within the recommended guidelines. Of course, the PIV software does not correlate on the mean flowfield but on instantaneous realizations of it, which are examined in Beresh et al. [2]. As part of that study, characteristic turbulent eddies comprising the jet interaction were computed by conditional ensemble averaging of the velocity fluctuation vector fields at the center of the strongest individual turbulent eddies. The resulting eddies of positive vorticity are reproduced in Fig. 12, from which a maximum velocity gradient of the eddy nearest x/d_j=33.8 can be calculated as about 2.0% of the interrogation window width. This result is appreciably larger than the maximum mean gradient of 0.4%, but is still well within the recommendations of Keane and Adrian [28] and Westerweel [14]. Nevertheless, Fig. 11b suggests that for this gradient strength, a measurable amount of negative bias error (in the range of 0.1 to 0.15 pixels) will occur in the turbulent stress for classical PIV algorithms – exactly what appears to be the case for the IDT results in Fig. 8a. Whereas past studies have shown the efficacy of the image deformation algorithm in extracting valid velocity vectors from regions of high velocity gradient in which classical PIV algorithms fail [17, 21, 23], the present results demonstrate that even where velocity vectors may be computed successfully by classical PIV, substantial bias errors may still occur. Fincham and Delerce [16], Scarano and Riethmuller [17], and Meunier and Leweke [22] provide some support for this observation, although none of these studies explicitly analyzes turbulence quantities as in the present work.

Additional biases can be expected when the velocity gradient does not simply vary linearly across an interrogation window [21-23, 29]. This influence was investigated by imposing a velocity gradient of exponential rather than linear character upon the simulated one-dimensional turbulence, that is, $du/dx=Ae^{Cx}$ rather than $du/dx=A$ as previously. The exponential constant C is always positive and is randomly chosen for each image pair from a one-sided Gaussian distribution of width σ_c. Velocities are compiled only near the center of the images and results are given in Fig. 13 for two values of the velocity gradient strength σ_g=1.0 and 2.0; synthetic images were created only for d_p=1.5 because Fig. 11b does not show a great dependence upon the particle image diameter. The mean velocities in Fig. 13a exhibit the characteristics of increased convergence error, particularly for the IDT results at σ_g=2.0. The error in the turbulent stress shown in Fig. 13b displays an escalation as soon as a nonlinear character of the velocity gradient is introduced, with a similar increase in error for both software packages though they may

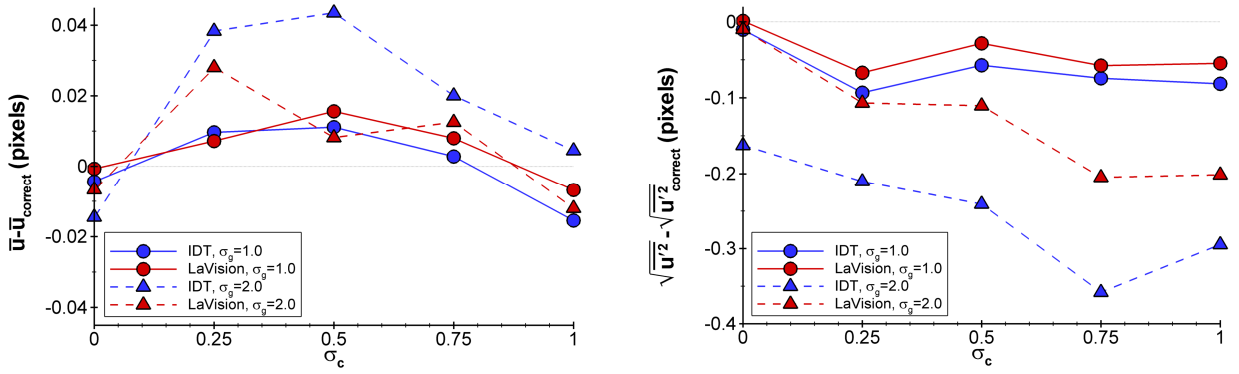

(a) **(b)**

Fig. 13: Error in synthetic PIV images of one-dimensional turbulence with an imposed velocity gradient of exponential rather than linear character, as a function of the magnitude of the gradient's exponential constant (σ_v =2.0, d_p=1.5). (a) mean velocity; (b) turbulent stress.

begin from different error levels. Even for σ_g=1.0, where the error is nearly zero when the gradient is linear (i.e., σ_c=0), significant errors arise as soon as a nonlinear gradient is introduced. This is true of both software packages, indicating that the LaVision image deformation algorithm is not adequate to fully treat such second-order velocity gradients.

In most practical situations, the nonlinear character of the velocity gradient over a reasonably sized interrogation window should be fairly mild, but nevertheless Fig. 13 establishes that this effect is an additional source of bias error. The maximum second derivative of the velocity (i.e., the variation of the velocity gradient) for the characteristic turbulent eddies of Fig. 12 was found to be about 1.0×10^{-5}. By way of comparison with Fig. 13b, when σ_c=0.25, the mean second derivative is about 0.8×10^{-5} for σ_g=1.0 and about 1.8×10^{-5} for σ_g=2.0. This suggests an increase in the turbulent stress bias error of perhaps 0.05 to 0.1 pixels as compared to the linear gradients simulations of Fig. 11. Although it lies beyond the intended scope of this study to thoroughly detail the nature of this particular velocity bias, Fig. 13 suffices to demonstrate that the nonlinear gradient effect will exaggerate the bias error in the turbulent stress as computed by the classical IDT software and in fact can induce error in the advanced LaVision algorithm as well.

The preceding analysis using the synthetic PIV tests suggests that for the 2-C PIV data of the jet-in-crossflow experiments, a negative bias in the turbulent stresses would occur for the classical PIV algorithm of the IDT software as compared to the advanced algorithm of the LaVision software, with a magnitude of about 0.15 pixels. This is less than the magnitude of the bias in Fig. 8a; given that U_∞ corresponds to a displacement of about 8 pixels in the 2-C data, the bias in $\overline{v'^2}$ equates to about 0.4-0.5 pixels of displacement. However, it is troublesome to precisely relate error computed from synthetic PIV to that found in real data, as the latter is subject to additional imperfections not simulated by the synthetic PIV and errors may be exacerbated by such factors as camera noise, laser sheet intensity variations, background illumination, camera fill factor, out-of-plane particle loss, etc. These effects might further contribute to differing results from advanced PIV algorithms such as image deformation as compared to classical analysis, and hence the preceding synthetic PIV analysis is more useful in determining the relevance of particular error sources than it is in establishing a precise magnitude that may be used for estimating measurement uncertainty.

Conclusion

Particle image velocimetry (PIV) data have been acquired using three different experimental configurations in the far-field of the interaction created by a supersonic axisymmetric jet exhausting transversely from a flat plate into a transonic crossflow. The measurement planes intersect at a common line, allowing a comparison of their results with respect to their estimated uncertainties for the components of the mean velocity and the turbulent stress tensor that are common to all configurations. Data acquired in a streamwise configuration, regardless of whether two-component measurements or stereoscopic measurements, showed agreement to within their respective uncertainties, but stereoscopic data from the crossplane exhibited a lower magnitude in the mean velocity and the turbulent stresses by a small but significant degree. Further investigation by reprocessing the data in nominally the same

manner but using a different software package revealed unrecognized error sources associated with the choice of software, which were well in excess of the earlier error estimates.

The discrepancies between the results from the two software packages were traced to the use of image deformation in the newer software, which synthetic PIV tests show yields a more accurate result when velocity gradients are present in the flow. The small discrepancy between the streamwise and crossplane measurements in the mean data vanished when using the new software, but the greatest difference was found in the turbulent stresses. Substantial biases towards lower values in the older, classical PIV software occurred both in the synthetic PIV and the real data even for velocity gradients that lie within the recommended limits for classical PIV. Some error may remain even in the advanced processing algorithm due to the presence of nonlinear velocity gradients, but nevertheless these observations support the importance of image deformation in the latest PIV processing techniques as compared to the longer-established classical PIV algorithms.

The present approach of comparing PIV results from multiple configurations and processing techniques allows an evaluation not just of the agreement in the data itself, but also of the accuracy of the uncertainty estimation. Given that most experiments cannot be expected to produce this degree of redundancy, it is useful to appreciate whether common error estimation processes can reflect the errors that may actually exist in the data. Unfortunately, the present study demonstrates that the bias errors found to dominate the results are decidedly nontrivial to predict beforehand, and therefore this comparison between varied PIV configurations and data reduction techniques suggests that routine methods of uncertainty quantification may not fully capture the error sources of an experiment.

References

[1] Beresh, S. J., Henfling, J. F., Erven, R. J., and Spillers, R. W., "Penetration of a Transverse Supersonic Jet into a Subsonic Compressible Crossflow," *AIAA Journal*, Vol. 43, No. 2, 2005, pp. 379-389.

[2] Beresh, S. J., Henfling, J. F., Erven, R. J., and Spillers, R. W., "Turbulent Characteristics of a Transverse Supersonic Jet in a Subsonic Compressible Crossflow," *AIAA Journal*, Vol. 43, No. 11, 2005, pp. 2385-2394.

[3] Beresh, S. J., Henfling, J. F., Erven, R. J., and Spillers, R. W., "Crossplane Velocimetry of a Transverse Supersonic Jet in a Transonic Crossflow," *AIAA Journal*, Vol. 44, No. 12, 2006, pp. 3051-3061.

[4] Samimy, M., and Lele, S. K., "Motion of Particles with Inertia in a Compressible Free Shear Layer," *Physics of Fluids A*, Vol. 3, No. 8, 1991, pp. 1915-1923.

[5] Melling, A., "Tracer Particles and Seeding for Particle Image Velocimetry," *Measurement Science and Technology*, Vol. 8, No. 12, 1997, pp. 1406-1416.

[6] Prasad, A. K., and Adrian, R. J., "Stereoscopic Particle Image Velocimetry Applied to Liquid Flows," *Experiments in Fluids*, Vol. 15, No. 1, 1993, pp. 49-60.

[7] Yoon, J. H., and Lee, S. J., "Direct Comparison of 2D PIV and Stereoscopic PIV Measurements," *Measurement Science and Technology*, Vol. 13, No. 10, 2002, pp. 1631-1642.

[8] Soloff, S. M., Adrian, R. J., and Liu, Z. C., "Distortion Compensation for Generalized Stereoscopic Particle Image Velocimetry," *Measurement Science and Technology*, Vol. 8, No. 12, 1997, pp. 1441-1454.

[9] Zang, W., and Prasad, A. K., "Performance Evaluation of a Scheimpflug Stereocamera for Particle Image Velocimetry," *Applied Optics*, Vol. 36, No. 33, 1997, pp. 8738-8744.

[10] Lawson, N. J., and Wu, J., "Three-Dimensional Particle Image Velocimetry: Error Analysis of Stereoscopic Techniques," *Measurement Science and Technology*, Vol. 8, No. 8, 1997, pp. 894-900.

[11] Van Doorne, C. W. H., Westerweel, J., and Nieuwstadt, F. T. M., "Measurement Uncertainty of Stereoscopic-PIV for Flow with Large Out-of-Plane Motion," *Particle Image Velocimetry: Recent Improvements: Proceedings of the EUROPIV2 Workshop*, 2004, pp. 213-227.

[12] Willert, C., "Stereoscopic Digital Particle Image Velocimetry for Application in Wind Tunnel Flows," *Measurement Science and Technology*, Vol. 8, No. 12, 1997, pp. 1465-1479.

[13] Wieneke, B., "Stereo-PIV using Self-Calibration on Particle Images," *Experiments in Fluids*, Vol. 39, No. 2, 2005, pp.267-280.

[14] Westerweel, J., "Fundamentals of Digital Particle Image Velocimetry," *Measurement Science and Technology*, Vol. 8, No. 12, 1997, pp. 1379-1392.

[15] Westerweel, J., "Theoretical Analysis of the Measurement Precision in Particle Image Velocimetry," *Experiments in Fluids*, Vol. 29, No. 7, 2000, pp. S3-S12.

[16] Fincham, A., and Delerce, G., "Advanced Optimization of Correlation Imaging Velocimetry Algorithms," *Experiments in Fluids*, Vol. 29, No. 7, 2000, pp. S13-S22.

[17] Scarano, F., and Riethmuller, M. L., "Advances in Iterative Multigrid PIV Image processing," *Experiments in Fluids*, Vol. 29, No. 7, 2000, pp. S51-60.

[18] Scarano, F., "Iterative Image Deformation Methods in PIV," *Measurement Science and Technology*, Vol. 13, No. 1, 2002, pp. R1-R19.

[19] Piirto, M., Eloranta, H., Saarenrinne, P., and Karvinen, R., "A Comparative Study of Five Different PIV Interrogation Algorithms," *Experiments in Fluids*, Vol. 39, No. 3, 2005, pp. 571-588.

[20] Christensen, K. T., "The Influence of Peak-Locking Errors on Turbulence Statistics Computed from PIV Ensembles," *Experiments in Fluids*, Vol. 36, No. 3, 2004, pp. 484-497.
[21] Huang, H. T., Fiedler, H. E., and Wang, J. J., "Limitation and Improvement of PIV, Part II: Particle Image Distortion, a Novel Technique," *Experiments in Fluids*, Vol. 15, No. 4-5, 1993, pp. 263-273.
[22] Meunier, P., and Leweke, T., "Analysis and Treatment of Errors Due to High Velocity Gradients in Particle Image Velocimetry," *Experiments in Fluids*, Vol. 35, No. 5, 2003, pp. 408-421.
[23] Lecuona, A., Nogueira, J., Rodriguez, P. A., and Acosta, A., "PIV Evaluation Algorithms for Industrial Applications," *Measurement Science and Technology*, Vol. 15, No. 6, 2004, pp. 1027-1038.
[24] Stanislas, M., Okamoto, K., Kahler, C. J., and Westerweel, J., "Main Results of the Second International PIV Challenege," *Experiments in Fluids*, Vol. 39, No. 2, 2005, pp. 170-191.
[25] Keane, R. D., and Adrian, R. J., "Optimization of Particle Image Velocimeters. Part 1: Double Pulsed Systems," *Measurement Science and Technology*, Vol. 1, No. 11, 1990, pp. 1202-1215.
[26] Lecordier, B., and Trinité, M., "Advanced PIV Algorithms with Image Distortion Validation and Comparison using Synthetic Images of Turbulent Flow," *Particle Image Velocimetry: Recent Improvements: Proceedings of the EUROPIV2 Workshop*, 2004, pp. 115-132.
[27] Astarita, T., and Cardone, G., "Analysis of Interpolation Schemes for Image Deformation Methods in PIV," *Experiments in Fluids*, Vol. 38, No. 2, 2005, pp. 233-243.
[28] Keane, R. D., and Adrian, R. J., "Theory of Cross-Correlation Analysis of PIV Images," *Applied Scientific Research*, Vol. 49, No. 3, 1992, pp. 191-215.
[29] Scarano, F., "Theory of Non-Isotropic Spatial Resolution in PIV," *Experiments in Fluids*, Vol. 35, No. 3, 2003, pp. 268-277.